Airborne Measurements of the Structure of Thermals

By D. H. Lenschow and P. L. Stephens, National Center for Atmospheric Research, Boulder, Colorade, U.S.A.

Presented at XVI OSTIV Congress, Châteauroux, France (1978)

Abstract
Detailed measurements of the structure of thermals were obtained from the NCAR Electra aircraft in the vicinity of Okinawa, Japan, during the Air Mass Transformation Experiment (AMTEX). The airplane flights were conducted in February 1978 in the convective boundary layer resulting from the large temperature contrast between the relatively warm water of the East China Sea and the cold arctic air from the Asian continent. The structure of thermals throughout the boundary layer (typically 1 to 2 km deep) is examined. Humidity was used as an indicator of thermals. The variables were high-passed filtered with a 5 km cutoff digital filter to eliminate mesoscale variations. Segments of the 5 minute (30 km length) horizontal flight legs with humidity greater than half the standard deviation of humidity fluctuations for that leg were defined as thermals. This was found to be a better indicator of thermals than temperature in the upper part of the boundary layer since the temperature in a thermal can become cooler than its environment near the top of the boundary layer. Using mixed layer scaling, the normalized thermal length scale and mean vertical velocity were found to scale with $^1/_3$ power of normalized height, while the temperature excess and number of thermals per unit length scaled with the $-^1/_3$ power of height in the free convection region of the surface layer. The velocity and temperature scaling agrees with free convection similarity predictions. Using these results in the equation for mean thermal updraft velocity, the magnitude of vertical pressure gradient term can be estimated. This term is found to be at least of the same order of magnitude as the buoyancy term. The divergence of vertical velocity variance within a thermal is found to be several times as large as the mean updraft advection term.

1. Introduction

Instrumented airplanes can be very successfully utilized to investigate the structure of thermals. They can be flown from within a few meters of the surface on up through the top of the convective boundary layer (or mixed layer) while measuring temperature, air velocity, humidity, turbulence intensity and other variables that may be modulated by thermals. The structure of thermals can then be investigated either by case studies of particular thermals, by compositing a number of thermals to obtain, by some averaging process, a better representation of a «typical» or average thermal (and departures from an average thermal), or by computing the statistical properties of a field of thermals as compared to their environment. Airplanes have the advantage of being able to penetrate a large number of thermals along random lines of intersection, but are generally too fast and unwieldy to be able to probe in detail a single thermal by repeated passes through it or by circling around within it. Therefore, in order to delineate the structure of a typical thermal, one must be able to extrapolate from measurements along random lines of intersection of thermals by means of some idealized model of thermals as was done, for example, by Vul'fson (1961) and by Frisch and Businger (1973). In this paper, we limit ourselves to the study of a field of thermals and its environment, disregarding the details of the structure and evolution of a typical or average thermal or its deviation form the average.

In an attempt to generalize the results presented here to a convective boundary layer of arbitrary depth and surface buoyancy flux, mixed layer scaling (Deardorff, 1970) has been used; i. e. velocity, temperature and length scales are obtained from the buoyancy parameter, the surface buoyancy and temperature flux and the depth of the convective (or mixed) layer. This imposes some assumptions on the measurements and restricts the generality of the results. First, we assume that horizontally averaged turbulent covariances in the boundary layer are horizontally homogeneous. Second, we assume that clouds do not significantly affect the dynamics of the boundary layer. Clouds can modify boundary layer structure either by heat released through water phase changes or by distortion of the buoyancy flux profile through radiative flux divergence.

Both of these assumptions are reasonable for the data set used for the analysis presented here. The measurements were obtained from the NCAR Electra aircraft flying over the East China Sea in February, 1975, during outbreaks of cold continental air over the Kuroshio (a warm, northward flowing ocean current) as part of the Air Mass Transformation Experiment (AMTEX). Details of the experiment and aircraft flight tracks are given by Lenschow and Agee (1976).

2. Thermal Indicators

Regardless of which data analysis techniques are to be used for investigating the structure of thermals, some indicator is needed to define a thermal. Some of the possibilities include threshold values of temperature, updraft velocity, humidity or turbulence intensity. Each of these has advantages and disadvantages; none is ideal under all circumstances. A positive temperature excursion clearly delineates thermals in the lower part of the convective layer. Furthermore, it is the primary driving force of the thermal and, in the lower part of the boundary layer, the temperature excess of a thermal is typically considerably larger than the level of turbulent fluctuations of temperature within or outside of a thermal (Manton, 1977). However, in the upper part of the boundary layer the temperature excess disappears and is replaced by a deficit (Arnold, 1976). Because of its inertia, the thermal can overshoot its static equilibrium level until stopped by the increased stability at the top of the mixed layer. It then falls back while entraining air from above the mixed layer, and becomes a part of the environmental air. Updraft velocity is the primary response of the thermal to the temperature excess and is the means by which surface layer properties are transported to the upper part of the convective mixed layer. Furthermore, it is the characteristic that makes thermal soaring possible. However, turbulent fluctuations of vertical velocity both within and outside of thermals (Manton, 1977) and smaller scale circulations within the thermals themselves (Frisch, et al., 1976) may be larger than the mean thermal updraft velocity. Therefore, in order to use updraft velocity, some averaging is necessary,

which makes the edges of the thermal less distinct and eliminates small intersected segments of thermals from consideration. The high level of turbulence intensity both inside and outside of a thermal may also cause difficulties in using turbulence intensity as an indicator except, perhaps, near the surface.

Over a moist surface, humidity is similar to temperature in the lower part of the convective boundary layer in that the humidity excess is typically considerably larger than the level of turbulent fluctuations of humidity. Furthermore, as Wyngaard, et al. (1978) have noted, temperature and humidity are very well correlated in the lower part of the convective boundary layer even to very small wavelengths. The temperature-humidity covariance is generated by the large negative gradients of temperature and humidity near the surface and dissipated only by molecular destruction at wavelengths of a few centimeters or less. Therefore, in the lower part of the boundary layer, temperature and humidity give almost identical results as thermal indicators.

Higher up in the boundary layer the humidity in a thermal continues to be greater than the environment since the mean humidity gradient remains negative Wyngaard, et al. 1978). This is a consequence of the humidity decreasing abruptly (in the usual situation) across the top of the mixed layer, in contrast to temperature, which increases across the top of the mixed layer. Thus, mixing of air from above into the mixed layer, (i. e. entrainment), which is mainly the result of thermals penetrating into the free air (Jensen and Lenschow, 1978), causes warming and drying of the mixed layer air. Therefore, the downwarm moving environmental air, which consists mainly of air from dissipated thermals, has been warmed to such an extent that it may, on the average, be warmer than the thermals in the upper part of the mixed layer. On the other hand, the entrain ment process tends to dry the air even more than if entrainment had not occurred and thereby accentuate the humidity difference between thermals and their environment. Thus, humidity remains an indicator of thermals throughout the mixed layer. For these reasons, humidity was used in this study.

3. Techniques of Analysis

In addition to thermal-scale variations in temperature, velocity, humidity, etc. along horizontal airplane flight paths, larger scale variations exist as well, even over a uniform ocean surface. Temperature and humidity, in particular, increase almost linearly along downwind flight paths because of the air mass modification process. This effect is removed by linearly detrending all of the data over each analyzed segment of the flight legs which is 300 s, or a distance of about 30 km.

On scales of several kilometers to severals tens of kilometers, satellite photographs and buoy observations (Lenschow and Agee, 1976; Burt and Agee, 1977) reveal organized convective activity over the AMTEX area in the form of cloud streets and mesoscale cellular convection. The satellite photographs also show a persistent vortex street extending downwind from Cheju-do.

These variations are removed by filtering the data with a Lanczos (1956) high pass digital filter with a cutoff wavelength of about 5 km. The weights are generated by the formula

$$w_k \equiv i - \frac{1}{2\pi}\left[\sin(2\pi\, \nu_c\, k)\cos(1/2\pi k/M)\right], \quad -M \leq k \leq M \quad (1)$$

where the subscript k identifies the weight, M is half the total number of weights minus one (M = 500 for this case), and ν_c is the half-power point in cycles per data interval. The cutoff wavelength was determined by a series of comparisons with various values of ν_c. A shorter cutoff filtered out contributions of very large thermals, while a longer cutoff seemed not sufficiently effective in removing larger scale variations.

Thermals were identified by requiring that humidity be equal to or greater than a threshold value, which was chosen to be half the standard deviation of humidity, σ_q, calculated from the entire 300s segment of filtered data. Furthermore, any segment – thermal or non-thermal – had to consist of at least 5 data points, which is about 25 m. Segments shorter than this were tabulated separately. Their total contribution consisted of from 2% to 8% of the total data points. Their contribution to the total fluxes and variances was an even smaller percentage. Figure 1 shows a schematic example of the application of these criteria to a humidity time series.

Figure 2 shows the combined effects of both filtering and setting a threshold humidity value. Both sets of plots are of the same part of the time series and consist of 400 samples (20 s) or 2 km from the total flight segment of 30 km. The mean and linear trend have been removed from the 30 km segment. This particular flight leg was flown at 1004 mb. which is about 135 m above the

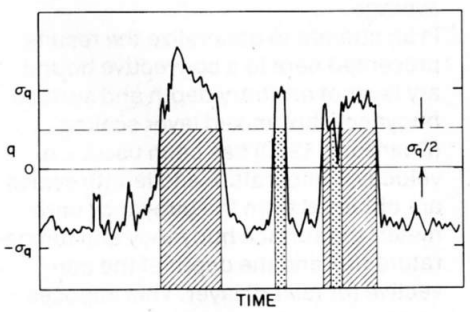

Fig. 1. A schematic example of the application of the threshold criteria for a thermal of 0.5 σ_q. Segments designated as thermals are cross-hatched. Segments less than 5 data points in length (25 m) are dotted; these are tabulated separately and make negligible contributions to the total statistics for the leg. The remainder is designated as non-thermals.

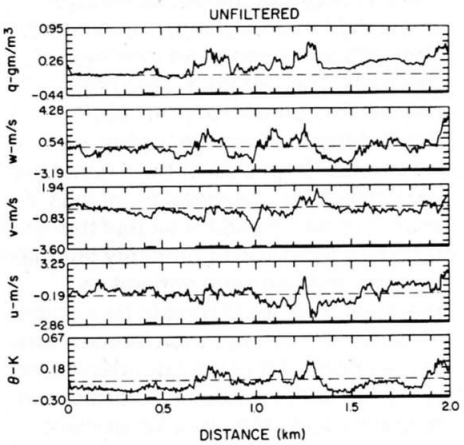

Fig. 2a. Unfiltered time series of absolute humidity (gm m^{-3}), vertical velocity, south wind component, east wind component and potential temperature for a 2 km segment of a 30 km flight leg. The mean and linear trend have been removed from the entire 30 km flight leg. Thermals, delineated by values of humidity greater than 0.5 σ_q, are indicated by the heavy line segments along the x-axis.

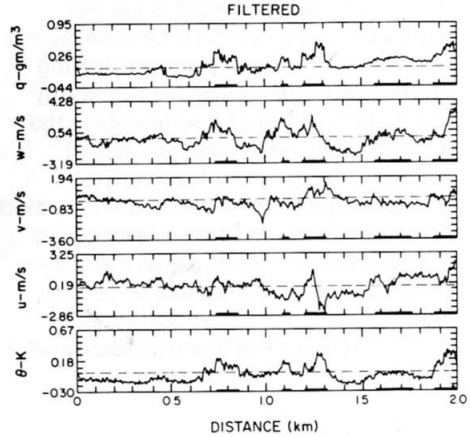

Fig. 2b. Same as Fig. 2a, except the variables are filtered with a 5 km wavelength cutoff high-pass digital filter.

surface. Thermals are quite apparent in both the humidity and temperature records, which are well correlated at this level. Figure 2a has not been filtered. Using $0.5\sigma_q$ as the threshold value of humidity, regions are classified as thermals which appear to be part of the environment; similarly, in other sections of the time series (not shown) thermals are classified as non-thermals because of larger scale variations in the time series. If the mean value of humidity had been used as an indicator, the entire segment would have been classified as a thermal. The segments classified as thermals in Fig. 2b, which consists of the filtered time series, are much closer to what one might identify as thermals on inspection of the time series.

The procedures outlined above may exclude actual portions of thermals, particularly the outside edges where entrainment reduces the humidity, as well as short intersected sections of thermals. Therefore, the criteria tend to underestimate the total area occupied by thermals. On the other hand, the thermal-designated segments have a high probability of actually being thermals. After subdividing the flight segments into thermal and non-thermal sections, values of variables characteristic of thermals and non-thermals are normalized, tabulated, averaged, and plotted. The mixed layer velocity and temperature scaling parameters,

$$w_* = (Q_{ov}\, z_i\, g/T)^{1/3}$$

$$\Theta_* = Q_o/w_*$$

where Q_{ov} is the surface virtual temperature flux, Q_o is the surface temperature flux, g/T is the buoyancy parameter, and z_i is the mixed layer depth, are used, along with z_i to scale the velocity and temperature excess, size and number of thermals. The results are then plotted on a normalized height scale to indicate the variations of the thermal properties with height. In this way, the results can be applied to any homogeneous convective boundary layer, regardless of its depth or degree of surface heating. This has been done for a large number of thermal and non-thermal properties (Stephens, 1978), including means and variances of temperature, velocity components and humidity, covariances of these quantities and third-order moments.

In the next section, we discuss the aircraft instrumentation and data recording system. Following this, we present the results for the mean values of temperature excess, updraft velocity, size and number of thermals.

4. Aircraft Instrumentation

The air velocity measurement system utilizes an inertial navigation system to measure the airplane velocity and angular orientation, and a gust probe mounted at the tip of a 6 m noseboom to measure the air velocity with respect to the airplane. Temperature fluctuations are measured with a 25 μm diameter platinum resistance wire thermometer, corrected for dynamic heating. Humidity fluctuations are measured with a Lyman-alpha hygrometer. Further details on the air motion sensing system are presented by Lenschow, et al. (1978). Temperature and humidity measurements on the Electra are discussed by Wyngaard, et al. (1978).

Most of the data were sampled and recorded digitally at 50 s^{-1}, which is reduced during processing to 20 s^{-1}. The variables are filtered with a 10 Hz 4-pole low-pass Butterworth filter.

5. Observational Results

The data used in this study were obtained from 6 of the NCAR Electra flights. Four of the flights were conducted during strong cold air outbreaks with northerly winds of to 15 m s^{-1}, surface virtual temperature fluxes of 0.13 to 0.24 K m s^{-1}, and a well-defined inversion at the top of the mixed layer. On the remaining 2 flights, winds were light from the south and east, air temperatures were warmer, the inversion was less pronounced, and the surface virtual heat flux was 0.08 to 0.10 K m s^{-1}. Flight levels varied from about 30 m to 1–2 km above the surface, depending upon the height of the inversion, which varied from 1200 to 1900 m. Measurements were obtained at from 2 to 5 levels on each of the different days. Since the lowest airplane flight level was typically at a height comparable to the absolute value of the Obhukov length (which varied from about 22 to 76 m), the lowest observation levels overlap the upper part of the surface layer (i.e. the free-convection layer). A common definition of the depth of the surface layer (e.g. Panofsky, 1978) is that part of the boundary layer $\leq 0.1\, z_i$. Many of the flight levels were above this height, so that mixed layer scaling of thermal variables is most appropriate.

Although scattered to broken stratocumulus clouds were present in the upper part of the mixed layer on all the flight days, they were usually thin and did not appear to be dynamically active. No precipitation was observed on any of the days. However, near the tops of the mixed layer the airplane may occasionally be in cloud, which can affect the accuracy of the humidity and temperature measurements. No obvious effects of wetting were noted, however. In any case, for the most part, cloud base was $>0.7\, z_i$.

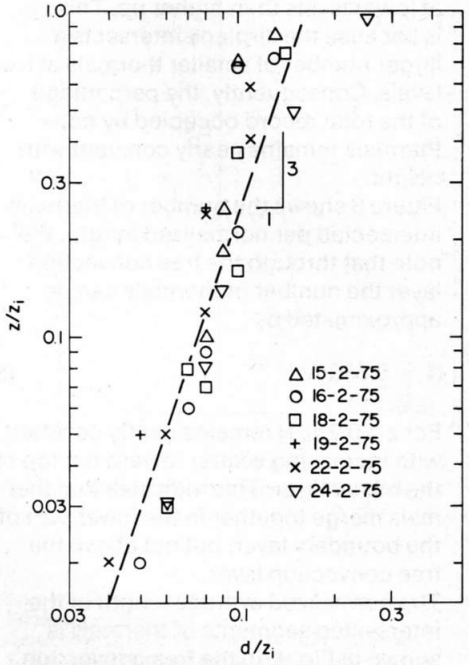

Fig. 3. Normalized average langth of the intersected segments of thermals.

The percentage of the total record occupied by thermals ranges from 20% to 30%, with a tendency to increase somewhat with height. Most of this increase is the result of the 5 sample (25 m length) restriction, which reduces the total record length of thermals more

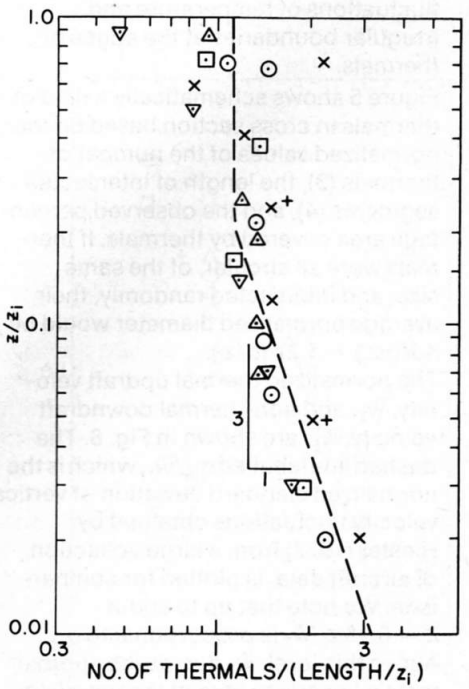

Fig. 4. Number of thermals intersected per normalized horizontal distance.

at lower levels than higher up. This is because the airplane intersects a larger number of smaller thermals at low levels. Consequently, the percentage of the total record occupied by non-thermals remains nearly constant with height.

Figure 3 shows the number of thermals intersected per normalized length. We note that through the free convection layer the number of thermals can be approximated by

$$N = 0.68(z/z_i)^{-1/3}. \quad (3)$$

For $z > 0.2\, z_i$, N remains nearly constant, with increasing scatter toward the top of the mixed layer. This indicates that thermals merge together in the lower part of the boundary layer, but not above the free convection layer.

The normalized average length of the intersected segments of thermals is shown in Fig. 4. In the free convection region, this length is given by

$$d/z_i = 0.161\,(z/z_i)^{1/3} \quad (4)$$

This relationship holds well above the free convection layer up to at least $z \cong 0.5\, z_i$. As noted previously, the minimum length of the intersected segments included in this compilation is 25 m, which excludes large numbers of short segments. Frisch and Businger (1973) and Manton (1977) found, for example, that most intersected segments (using temperature as an indicator) were less than 10 m width. Many of these short segments are likely due to turbulent fluctuations of temperature and irregular boundaries at the edges of thermals.

Figure 5 shows schematically a field of thermals in cross section based on the normalized values of the number of thermals (3), the length of intersected segments (4), and the observed percentage area covered by thermals. If thermals were all circular, of the same size, and intersected randomly, their average normalized diameter would be $4d/(\pi z_i) = 1.27\,(d/z_i)$.

The normalized thermal updraft velocity, $\bar{w}_T$, and non-thermal downdraft velocity, $\bar{w}_E$, are shown in Fig. 6. The dashed line labelled $\sigma_w/\bar{w}_*$, which is the normalized standard deviation of vertical velocity fluctuations obtained by Hiester (1977) from a large collection of aircraft data, is plotted for comparison. We note that up to about $Z = 0.15\, z_i$, $\bar{w}_T$ is proportional to σ_w. Above this level, $\bar{w}_T$ decreases approximately linearly to zero at the top of the mixed layer, while σ_w peaks at about

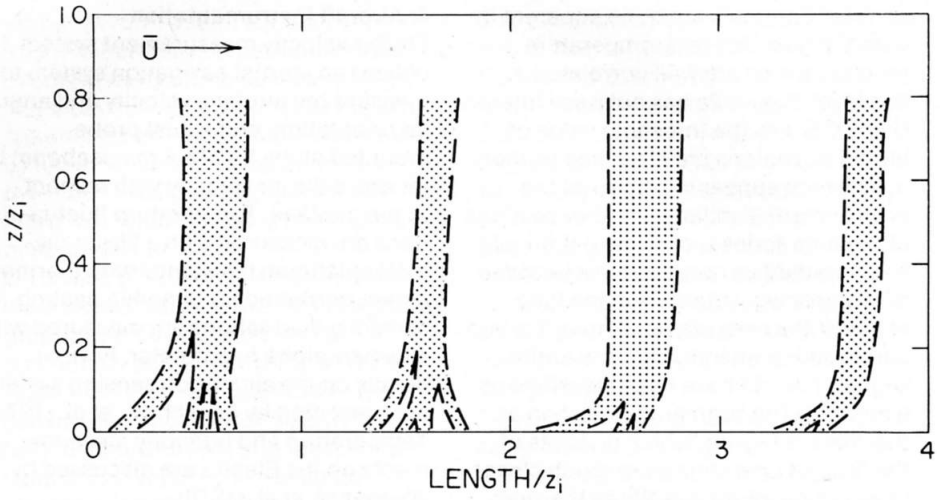

Fig. 5. Schematic cross-section of the boundary layer showing a field of thermals based on the size and number of thermals observed along the aircraft flight paths.

$0.4\, z_i$ and decreases slowly to about 66% of its peak value at the top of the mixed layer. The updraft velocity is plotted on a logarithmic scale in Fig. 7, which indicates that the updraft velocity in the free convection layer is given by

$$\bar{w}_T/w_* = 1.00\,(z/z_i)^{1/3}. \quad (5)$$

Manton (1977), using temperature as an indicator, obtained a value of 0.70 for the constant in (5). His method (also used by Frisch and Businger, 1973) of selecting a threshold value of temperature was less restrictive, however. By his criteria, thermals covered 43% of the total area.

On an individual thermal basis, (4) and (5) indicate that in the free convection layer the mass flux per thermal (updraft velocity times area) is proportional to z/z_i. Thus, the convergence is constant with height. The rate of change of momentum per thermal is proportional to $(z/z_i)^{1/3}$.

The normalized temperature deviation of a thermal is plotted in Fig. 8. The normalized standard deviation of temperature fluctuations (Hiester, 1977) is also plotted for comparison. We see that above about $0.5\, z_i$, the temperature in a thermal is less than the environment; i.e. a thermal is negatively buoyant through the upper half of the mixed layer. In the free convection layer, Fig. 9 indicates that the temperature excess is given by

$$\bar{\theta}_T/\Theta_* = 1.44\,(z/z_i)^{-1/3}. \quad (6)$$

Manton (1977) and Businger and Frisch (1973) obtained a value of about 1.9 for the constant in (6).

6. Vertical Equation of Mean Motion

The results in the previous section can be used to examine the dynamics of thermals. The vertical equation of mean motion averaged across a steady-state thermal (Tennekes and Lumley, 1972) can be written as

$$\bar{u}_T \frac{\delta \bar{w}_T}{\delta x} + \bar{v}_T \frac{\delta \bar{w}_T}{\delta y} + \frac{\delta \overline{u_T' w_T'}}{\delta x} + \frac{\delta \overline{v_T' w_T'}}{\delta y} + \bar{w}_T \frac{\delta \bar{w}_T}{\delta z} + \frac{\delta \overline{w_T'^2}}{\delta z} = -\frac{1}{\varrho}\frac{\delta \bar{P}_T}{\delta z} + \frac{g}{\Theta_o}\bar{\Theta}_T \quad (7)$$

where u_T', v_T' and w_T' are the turbulent velocity fluctuations within a thermal, Θ_o is the average potential temperature, ϱ is the air density, and $\bar{P}_T$ is that part of the pressure remaining after substracting the static pressure of the reference state, which obeys the hydrostatic condition,

$$\frac{\delta \bar{P}_{T_o}}{\delta z} = -g\varrho_o.$$

The first 4 terms in (7) express mainly the contribution of the entrainment of air through the sides of the thermal and, since the mean vertical velocity outside a thermal is less than zero, act as a drag on the upward motion of the thermal.

In the free convection layer, we can substitute (5) and (6) into (7). From the results presented by Stephens, (1978) we find that

$$\overline{w_T'^2}/w_*^2 = 2.72\,(z/z_i)^{2/3}. \quad (8)$$

Solving (7) for the remaining unknown terms, we have

$$E + \frac{1}{\varrho}\frac{\delta \bar{P}_T}{\delta z} = \frac{g}{\Theta_o}\bar{\Theta}_T - \bar{w}_T \frac{\delta \bar{w}_T}{\delta z} - \frac{\delta \overline{w_T'^2}}{\delta z}. \quad (9)$$

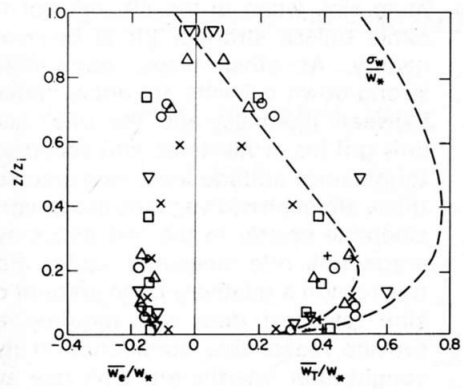

Fig. 6. Mean updraft velocity in thermals and downdraft velocity in the environment. The 2 values in parentheses near the top of the mixed layer have been multiplied by −1 and plotted as positive thermal updraft and negative environmental downdraft velocities.

where E is the entrainment term. Normalizing (9), the terms on the right-hand side are

$$[1.44 - 0.33 - 1.82]\ (z/z_i)^{-1/3} =$$

$$-.0.71(z/z_i)^{-1/3}$$

Since E >0,

$$\left(\frac{z_i}{w_*^2}\right)\frac{1}{\varrho}\frac{\delta \bar{P}_T}{\delta z} < -0.71\ (z/z_i)^{-1/3}. \qquad (10)$$

From this we see that in the free convection layer the pressure term is at least of the same order of magnitude as the other terms and acts to accelerate the thermal. This agrees with the results of Kaimal and Businger (1970) who integrated the vertical equation of motion between 2 tower levels in the surface layer. We also note that the divergence of the variance of vertical velocity in a thermal is several times larger than the mean updraft velocity term.

7. Conclusions

Aircraft observations over a relatively warm ocean surface have been used to study the structure of thermals, using a threshold value of humidity as an indicator of thermals. Humidity is found to have several advantages over temperature and updraft velocity as a thermal indicator, particularly in the upper part of the mixed layer. We find that thermal updraft velocity, temperature deviation, and size and number of thermals can be normalized with mixed layer scaling parameters to collapse the data onto single curves from the upper part of the surface layer to the top of the mixed layer. In the free convection layer, the curves follow predictions of Monin-Obukhov free-convection similarity theory.

On the basis of these results, we can estimate many of the terms in the equation of mean updraft velocity of a thermal. We conclude that in the free convection layer, the pressure gradient term is at least of similar magnitude as the buoyancy term and acts to accelerate the thermal. The divergence of the vertical velocity variance is several times as large as the mean updraft advection term.

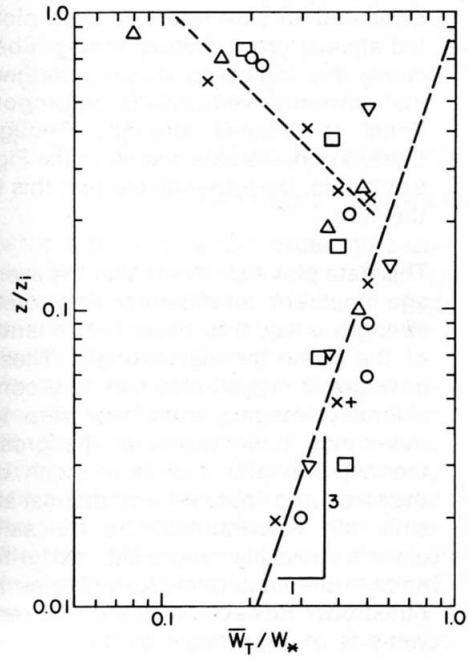

Fig. 7. Mean thermal updraft velocity.

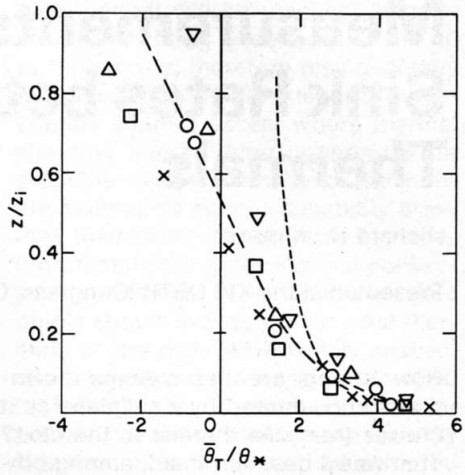

Fig. 8. Mean temperature deviation of thermals.

References

Arnold, A.: A lapse rate depiction for clear air convection. J. Appl. Meteor. 15, 1976.

Burt, W. V. and E. M. Agee,: Buoy and satellite observations of mesoscale cellular convection during AMTEX '75, Boundary-Layer Meteorol. 12, 1977.

Deardorff, J. W.: Convective velocity and temperature scales for the unstable planetary boundary layer and for Rayleigh convection. J. Atmos. Sci. 27, 1970.

Frisch, A. S., R. B. Chadwick, W. T. Moninger and J. M. Young: Observations of boundary layer convection cells measured by dualdoppler radar and echosonde, and by microbarograph array. Boundary-Layer Meteorol., 3, 1976.

Frisch, A. S., and J. A. Businger: A study of convective elements in the atmospheric surface layer. Boundary-Layer Meteorol. 3, 1973.

Hiester, T. R.: Parameterization of the unstably stratified planetary boundary layer using aircraft data. M. S. Thesis, University of Washington, Seattle, 1977.

Jensen, N. O. and D. H. Lenschow: A observational investigation of penetrative convection. J. Atmos. Sci. (Accepted for publication) 1978.

Kaimal, J. C. and J. A. Businger: Case studies of a convective plume and a dust devil. J. Appl. Meteorol. 9, 1970.

Lanczos, C.: Applied Analysis. Prentice Hall, Inc., Englewood Cliffs, N. J., 1956.

Lenschow, D. H., C. A. Cullian, R. B. Friesen and E. N. Brown: The status of air motion measurements on NCAR aircraft. Fourth Symposium on Meteorological Observations and Instrumentation, Apr. 10–14, 1978.

Lenschow, D. H. and E. M. Agee: Preliminary results from the Air Mass Transformation Experiment (AMTEX). Bull. Amer. Meteor. Soc. 57, 1976.

Manton, M. J.: On the structure of convection. Boundary-Layer Meteorol. 12, 1977.

Panofsky, H. A.: Matching in the convective planetary boundary layer. J. Atmos. Sci., 35, 1978.

Stephens, P. L.: The role of thermals in the turbulence processes of the convective boundary layer. M. S. Thesis, University of Oklahoma. 1978.

Tennekes, H. and J. L. Lumley: A First Course in Turbulence. Cambridge, Massachusetts, The MIT Press, 1972.

Vul'fson, N. E.: Convection Motions in a Free Atmosphere, Israel Program for Scientific Translations, Jerusalem, 1961.

Wyngaard, J. C., W. T. Pennell, D. H. Lenschow and M. A. LeMone: The temperature-humidity covariance budget in the convective boundary layer. J. Atmos. Sci. 35, 1978.

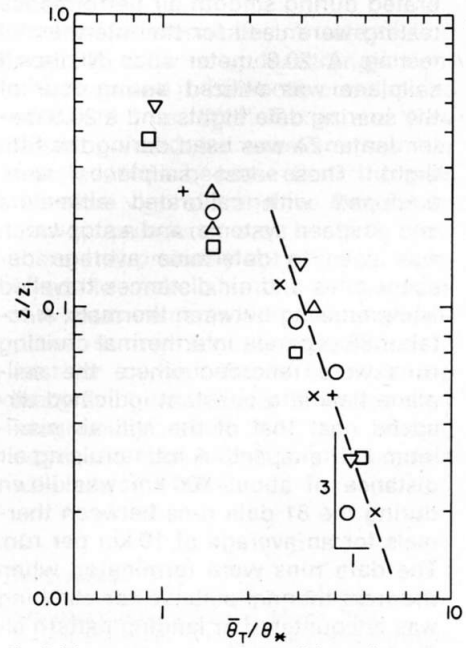

Fig. 9. Mean temperature excess of thermals.